Astron. Astrophys. 348, 466–474 (1999)

ASTRONOMY
AND
ASTROPHYSICS

The orbital period of the dwarf nova HS Virginis, the revised $P_o - P_s$ relation and the "superhump" mass ratio distribution of SU UMa stars⋆

R.E. Mennickent[1,⋆⋆], **K. Matsumoto**[2], **and J. Arenas**[3]

[1] Universidad de Concepción, Departamento de Física, Casilla 4009, Concepción, Chile (rmennick@stars.cfm.udec.cl)
[2] Kyoto University, Faculty of Science, Department of Astronomy, Kyoto 606-8502, Japan (katsura@kusastro.kyoto-u.ac.jp)
[3] Keele University, Department of Physics, Keele, Staffordshire ST5 5BG, UK (jla@astro.keele.ac.uk)

Received 17 March 1999 / Accepted 4 June 1999

Abstract. A spectroscopic study of the SU UMa star HS Vir is presented. From the analysis of the radial velocities of the Hα emission line the most likely orbital period is $0^{\rm d}.07692(3)$, although we cannot discard two aliases at $0^{\rm d}.07678$ and $0^{\rm d}.07709$. The Balmer lines follow the orbital period with a radial velocity semiamplitude $K = 96 \pm 9\,{\rm km\,s^{-1}}$, but the He I λ 5875 emission line shows a double wave during the orbital cycle. We found that the mean Balmer, He I and He II 4686 lines can be roughly modeled with a disk radial emissivity $\propto r^{-2}$. A revised version of the $P_o - P_s$ relation for SU UMa stars is also given, which is relevant for discriminating between $\pm$ 1 c/d aliases of the orbital period. We calculated the mass ratio, derived from the tidal resonance model, of HS Vir (q_{sh} = 0.22 $\pm$ 0.04) and 43 additional SU UMa stars. The q_{sh} distribution has a roughly gaussian shape with a mean 0.14, in sharp contrast with the orbital period distribution. Finally, a discussion of the possible stellar masses and inclination of HS Vir is given. We observe that the mass ratio derived from the dynamic solution is in disagreement with that derived from the tidal resonance model. This fact probably indicates that K does not represent the white dwarf binary motion.

Key words: stars: individual: HS Vir – stars: novae, cataclysmic variables – stars: fundamental parameters – stars: evolution – stars: binaries: general

1. Introduction

HS Vir (also referred as PG 1341-079, $\alpha_{2000} = 13^h43^m38^s.5$, $\delta_{2000} = -08^o14'04''$, Ritter & Kolb 1998) was classified as a genuine member of the SU UMa-type dwarf novae after the discovery of superhumps during the 1996 March superoutburst (Kato et al. 1998). These authors found superhumps with a mean period of $0^{\rm d}.08059(3)$ decreasing at rate $\dot{P}/P$ = -4(1) $\times 10^{-5}$ as usually observed in SU UMa stars (for a review of SU UMa stars and cataclysmic variables see Warner 1995a, 1995b).

Kato et al. (1998) also reviewed previous photometric observations of HS Vir, observing that the short recurrence time (8 d) and the smallness of outburst amplitude (2.7 to 3.5 mag) resemble that found in ER UMa stars (Kato et al. 1995, Misselt & Shafter 1995, Robertson et al. 1995, Nogami et al. 1995, Kato et al. 1996). However, the suspected supercycle length (longer than 80 d) and the slow speed of the rapid decline stage ($\sim 0^{\rm m}.5$ ${\rm d^{-1}}$, compared with ≥ 1 mag ${\rm d^{-1}}$ of most SU UMa stars) make the star unique among SU UMa stars.

The only previous spectroscopic study of HS Vir is by Ringwald (1993). He found double peaked Hα emission and a strong S-wave in his low resolution spectra. Based on 32 radial velocities, he found an orbital period of $0^{\rm d}.0836$, although the shorter one-day alias ($0^{\rm d}.077$) is favored by the superhump period (Kato et al. 1998).

This paper is aimed at solving the controversy about the orbital period and discusses possible system parameters of HS Vir. We also give the disk radial line emissivity under some basic assumptions.

2. Observations and data reduction

The observations were conducted at the 3.5 m NTT telescope of La Silla, ESO during two runs on April and May 1998. The CCD # 36 and grating # 8 combined with a slit width of one arcsecond yielded a spectral resolution of 2.5 Å (114 km s^{-1} at Hα) and a spectral range of $\lambda\lambda$ 4450–7025 Å. The slit was always rotated to the parallactic angle to correct for losses due to atmospheric refraction. He-Ar comparison images were taken typically in intervals of 30 minutes between several 5 m science exposures. Additional calibrations like Flat Fields and Biases were taken during day time. The observations are summarized in Table 1.

Image reductions were realized in the usual manner. First, the two dimensional frames were divided by the normalized Flat

Send offprint requests to: R.E. Mennickent

⋆ Based on observations obtained at ESO La Silla Observatory (ESO Proposal 61.D-0395).

⋆⋆ On leave in Harvard-Smithsonian Center for Astrophysics, 60 Garden St, MA 02138, Cambridge, USA

Table 1. Summary of observations. The number of spectra N and the HJD (-2450 900) at the start and end of the night are given.

Date(UT)	N	HJD_{start}	HJD_{end}
16/04/98	32	20.7369	20.8928
17/04/98	39	21.6757	21.8744
18/04/98	20	22.5124	22.6103
19/04/98	15	23.6710	23.8130
20/04/98	20	24.5239	24.8504
29/05/98	13	63.7024	63.7615
30/05/98	18	64.6794	64.7662
31/05/98	34	65.5414	65.7487

Field subtracting also the Bias using the IRAF[1] *ccdproc* routine. After that, one dimensional spectra were extracted (subtracting the sky) and wavelength calibrated using the IRAF *doslit* package. About 40 He-Ar emission lines provided spectral calibration functions with typical rms of 0.4 Å (18 km s^{-1} at Hα). As a measure of the internal accuracy and stability of our wavelength calibration, we measured the radial velocity of the atmospheric band at λ 6870–6875 deblending the line with two gaussians of variable center and width. The rms of the velocity distributions were about 20 km s^{-1} with the same mean value every night.

We realized several measures in the calibrated spectra. The peak separation was measured after deblending the emission profile with two gaussians of variable sizes and center. The equivalent width was measured integrating the line flux between the points where the line wings intersect the continuum level. At the same intensity, the full width at zero intensity ($FWZI$) was measured. Sometimes, in blended lines (like He I λ 4921) we measured the half width at zero intensity with respect to the central depression and then, assuming a symmetric profile, we measured $FWZI$. Except for these cases, the measures were made automatically using the *bplot* IRAF task. In addition, as a measure of the line strength, the intensity ratio $\Theta \equiv (I_{\lambda}^{max} - 1)/(I_{\alpha}^{max} - 1)$ was measured interactively with the cursor. Sources of errors are the profile's S/N ratio, continuum normalization and λ calibration. In general they are of the order of 5% or less.

Radial velocities (RVs) of the emission lines, referred to the Local Standard of Rest (V_{sun} = 20 km s^{-1}, $\alpha_{sun} = 18^h$ and $\delta_{sun} = +30^o$), were measured using the algorithm originally developed by Schneider & Young (1980), adopted by Shafter (1983) and refined by Horne et al. (1986). This method provides a robust diagnostic test to investigate the behavior of different profile sections during the orbital cycle. The method simultaneously shifts two gaussians of standard deviation σ_g (or alternatively full width at half maximum $FWHM_g$) and separation Δ along the emission profile until a velocity is found for which the convolved flux in both is the same. Changing Δ and $FWHM_g$ we can probe different velocity sections of every profile.

[1] IRAF is distributed by the National Optical Astronomy Observatories, which are operated by the Association of Universities for Research in Astronomy, Inc., under cooperative agreement with the National Science Foundation

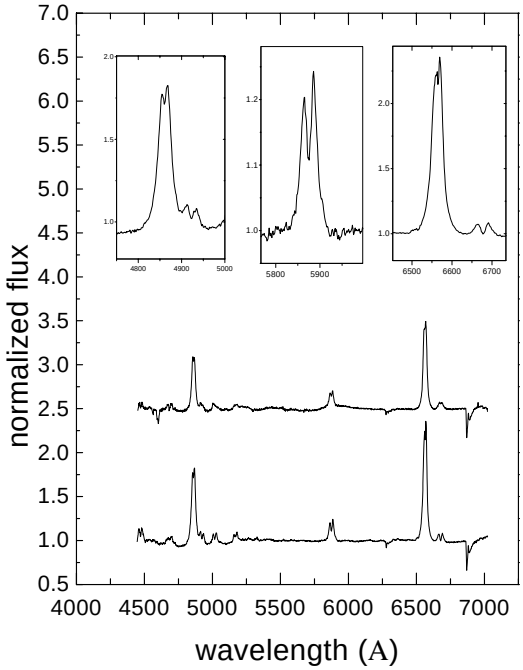

Fig. 1. The normalized mean spectra during April (*down*) and May (*up*) 1998. The May spectrum is vertically shifted by 1.5 continuum units. A closer look of the main emission lines is also shown in the upper graphs. The absorption features at $\lambda\lambda$ 4564 and 4602 Å on May 1998 are residuals of the reduction process.

For the low S/N emission lines (like He I 5875) the centroid method was preferred to the double gaussian technique. This way we waive to document the RV changes at different sections of the emission profile but we gain accuracy as the method involves all the line pixels.

We searched for periods in the RV data sample using the Scargle (1982) method and tested our results with the *pdm* (phase dispersion minimization, Stellingwerf 1978) algorithm incorporated in IRAF, and with a simple Fourier transform implemented in the Period98 software (Sperl 1998). The range of frequency scanned was between the Nyquist frequency, i.e. 1.7 $\times 10^{-3}$ c/d and 1 c/d.

3. Results

3.1. The averaged spectrum and variability

The mean spectra of HS Vir during April and May 1998 are shown in Fig. 1. They show broad double emissions of neutral hydrogen and helium, typical signatures of accretion disks rotating at supersonic velocities. A flat Balmer and He I decrement is observed, as usual in CVs (Williams and Ferguson 1982, Ferguson 1997). The ratio between the HeI triplet ($\lambda\lambda$ 5875, 4471) and singlet ($\lambda\lambda$ 6678, 4921) is about 2, just in the middle of the optically thin and optically thick cases discussed by Williams and Ferguson (1982). We note that He II 4686 is double peaked rather than single peaked, more consistent with an origin in a disk's chromosphere that in a wind as suggested by Hoare (1994).

Table 2. Spectroscopic measures of the spectra shown in Fig. 1. April and May values are separated by a slash. a, sp and c indicate absent, single peak and asymmetrical blended profile, respectively. The typical error is 5%. We show the ratio Θ between line and Hα maximum intensity (see text) except for Hα where the reference level for Θ is the continuum. The peak separation (Δ_λ) and the full width at zero intensity ($FWZI$) are also shown.

Line	Θ	$\Delta_\lambda(km\,s^{-1})$	$FWZI(km\,s^{-1})$
He I 4478	0.1/0.07	1560/1290	3610/2820
He II 4686	0.03/0.06	1690/1700	3265/3360
Hβ	0.61/0.60	670/590	5305/5555
He I 4921	0.06/0.07	1330/sp	2707/c
He I 5016	0.06/0.06	1390/sp	2870/3470
Fe II 5169	0.07/0.05	1230/sp	2970/c
He I 5875	0.18/0.21	1260/1040	4310/3100
Hα	2.35/1.99	360/sp	6130/5260
O I 6351	0.02/a	1420/a	2590/a
He I 6678	0.06/0.07	1280/780	3280/3550

The most prominent lines, Hα and Hβ, are characterized by equivalent widths ~ -40 Å, and peak separation ~ 500 km s^{-1}. In contrast, the helium lines ($\lambda\lambda$ 4471, 6678 Å along with 4921 and 5016 Å possibly blended with Fe II 4924 and 5018 Å) are weaker, with equivalent widths between -3 and -9 Å, and much larger peak separation, about 1200 km s^{-1}. The weaker lines at λ 6351, 5169 and 4686 probably correspond to O I, Fe II and He II respectively. The He II 4686 to Hβ intensity ratio is $\sim$ 0.05, a normal value among dwarf novae (Echevarría 1988).

Besides a 25% decrease of the mean emission strength between April and May 1998, the spectra show basically the same features during both seasons. The variability of the Balmer lines amount to 10% (std) of the mean, whereas He 5875 varied by about 25%. After folding the emission line equivalent width with the binary phase no phase dependent variation was observed. Mean spectroscopic parameters are given in Table 2.

3.2. The orbital period and radial velocity semiamplitude

A set of Hα radial velocities was obtained with $FWHM_g = 8$ Å and Δ = 40 Å. The results, shown in Table 3, show the radial velocities during the first night of May shifted by about 100 km s^{-1} with respect to the other 7 nights (the same effect is observed in the Hβ line). This is a real effect which cannot be an instrumental effect (for example the earth's lines did not show this shift). These 13 spectra were not used for the period search neither for the subsequent K diagnostic diagrams.

A search for the orbital period was done applying the Scargle's statistics (implemented in the AVE package; http://www.gea.cesca.es) to the data set of Table 3. This statistics obeys an exponential probability distribution and is especially useful for smooth oscillations. The false alarm probability p_0 depends on the periodogram's power level z_0, viz. $z_0 \approx \ln N/p_0$, for small p_0, where N is the number of frequencies searched for the maximum power (Scargle 1982, Eq. 19). The periodogram shown in Fig. 2 was obtained with N = 7500, so the 99% confidence level (i.e. those corresponding to p_0 = 0.01) corresponds to z_0 = 13.5.

Table 3. Radial velocities (in km s^{-1}) of the Hα emission line versus HJD (- 2450 900)

HJD	v	HJD	v	HJD	v	HJD	v
20.7369	-46	21.7568	36	23.6926	52	64.7015	202
20.7422	-37	21.7611	45	23.6970	78	64.7120	132
20.7486	33	21.7654	62	23.7013	105	64.7163	156
20.7529	70	21.7698	39	23.7861	232	64.7209	82
20.7573	57	21.7742	103	23.7913	156	64.7252	59
20.7631	61	21.7785	124	23.7956	80	64.7295	-22
20.7675	99	21.7829	159	23.8000	-11	64.7338	-32
20.7719	130	21.7898	131	23.8043	-37	64.7448	122
20.7762	129	21.8081	-23	23.8087	-93	64.7491	0
20.7859	109	21.8124	-54	23.8130	-124	64.7533	43
20.7906	74	21.8167	-33	24.5239	80	64.7576	44
20.7949	23	21.8211	-8	24.5282	-8	64.7619	-185
20.7995	7	21.8255	48	24.5326	0	64.7662	70
20.8038	-45	21.8298	-42	24.5369	51	65.5414	102
20.8082	-26	21.8342	-22	24.5412	139	65.5457	139
20.8125	-29	21.8438	4	24.5455	59	65.5499	112
20.8208	-19	21.8482	50	24.5498	111	65.5597	86
20.8251	-47	21.8526	74	24.5542	146	65.5640	153
20.8294	-40	21.8570	97	24.5644	117	65.5734	-34
20.8338	-13	21.8614	115	24.5738	45	65.5777	-60
20.8382	-48	21.8658	71	24.5781	-26	65.5819	-102
20.8425	26	21.8701	40	24.5825	-71	65.5862	-117
20.8469	128	21.8745	-2	24.5868	-56	65.5906	-61
20.8512	140	22.5124	-67	24.5911	-40	65.5948	-19
20.8615	130	22.5167	-44	24.5954	21	65.6406	-8
20.8659	129	22.5211	13	24.5998	27	65.6448	23
20.8703	82	22.5254	1	24.6041	51	65.6491	-47
20.8747	116	22.5297	55	24.8422	-17	65.6535	-66
20.8796	96	22.5341	88	24.8465	12	65.6622	-57
20.8840	49	22.5385	82	24.8508	57	65.6673	-22
20.8884	-2	22.5427	80	63.7024	215	65.6720	9
20.8928	-14	22.5548	140	63.7070	242	65.6763	46
21.6757	113	22.5593	158	63.7113	240	65.6806	87
21.6801	-20	22.5636	107	63.7157	145	65.6849	129
21.6845	-26	22.5679	54	63.7200	144	65.6892	159
21.6887	6	22.5724	23	63.7242	155	65.6942	106
21.6930	37	22.5767	16	63.7285	115	65.7003	170
21.6980	69	22.5811	-38	63.7400	151	65.7046	50
21.7023	108	22.5854	-54	63.7443	172	65.7089	194
21.7066	98	22.5973	44	63.7486	129	65.7133	23
21.7164	21	22.6016	82	63.7529	149	65.7176	-72
21.7211	-6	22.6060	107	63.7572	194	65.7274	-108
21.7254	-72	22.6103	109	63.7615	183	65.7317	-56
21.7297	-44	23.6710	-30	64.6794	-9	65.7360	-143
21.7341	-64	23.6753	-2	64.6837	53	65.7402	-41
21.7385	-66	23.6796	16	64.6886	-44	65.7445	-21
21.7428	-64	23.6839	-17	64.6930	15	65.7487	23
21.7472	-63	23.6882	-3	64.6973	62		

Fig. 2 shows a strong period at $0^{\rm d}.07692(3)$ with two aliases of lower power at $0^{\rm d}.07678$ and $0^{\rm d}.07706$. This result was confirmed applying the *pdm* and Fourier methods. We cannot completely rule out the two aliases based on their lower significance,

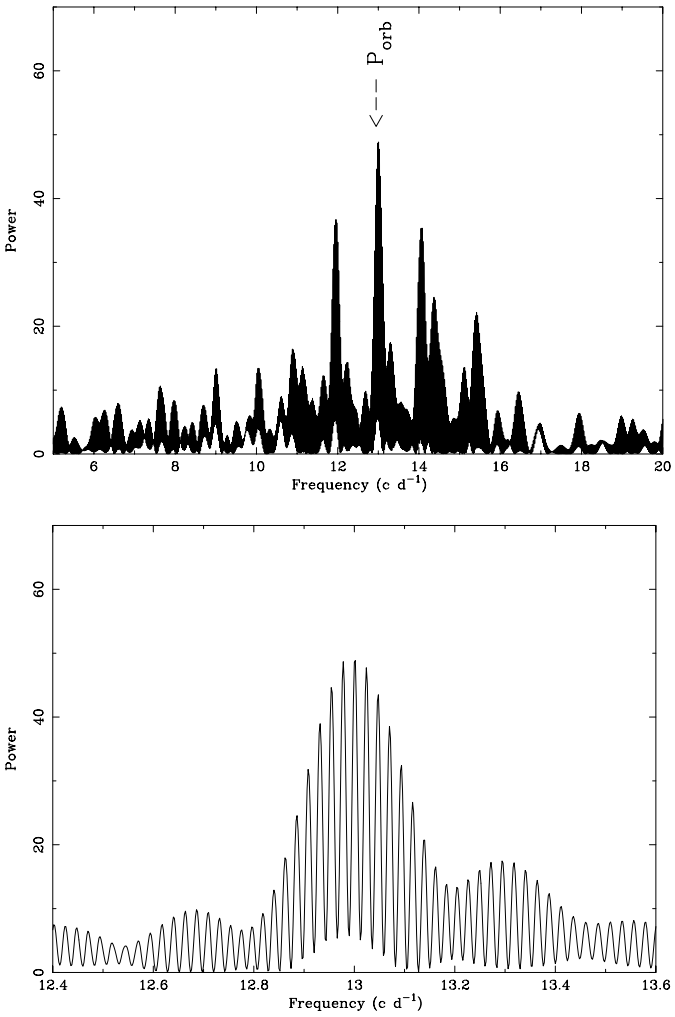

Fig. 2. *Up:* The Scargle periodogram for the Hα radial velocities of Table 3. The central peak at $0\overset{\mathrm{d}}{.}07692$ (13.00 c d^{-1}) is flanked by the $\pm$ 1 c d^{-1} aliases at $0\overset{\mathrm{d}}{.}071$ and $0\overset{\mathrm{d}}{.}083$. The 99% confidence level is at power 13.5. *Below:* A zoom into the region of maximum power.

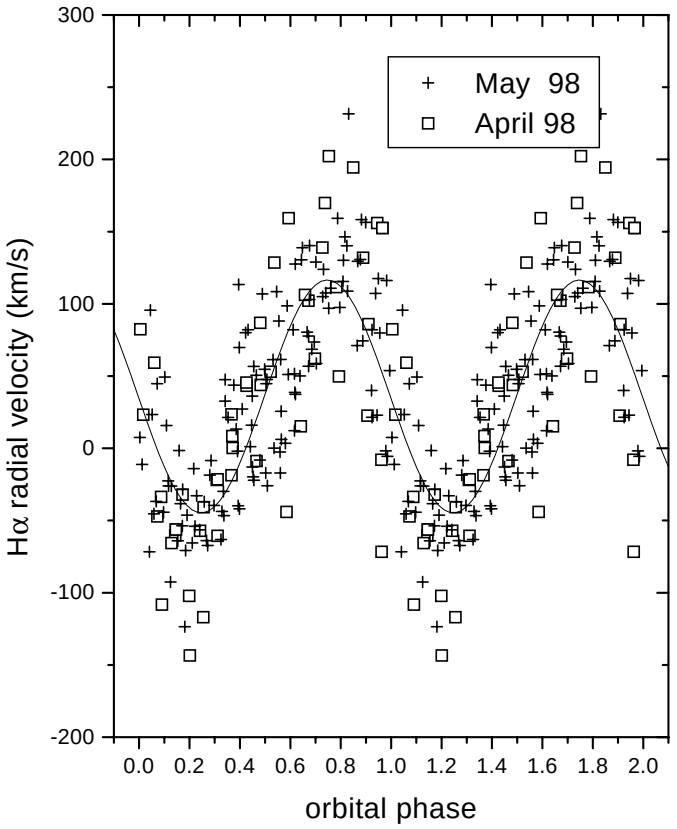

Fig. 3. The Hα radial velocities of Table 3 folded with the orbital period $0\overset{\mathrm{d}}{.}07692$. The best sinusoid fit is also shown.

but the periodogram is probably symmetrical with respect to the true period, favoring the $0\overset{\mathrm{d}}{.}07692$ period. Adding the Ringwald (1993) data to our analysis did not improve the period accuracy neither solve the aliasing problem.

The ephemeris for the time when the RV $-\,\gamma$ changes from positive to negative is:

$$T = 2450920.72229(77) + 0\overset{\mathrm{d}}{.}07692(3)E \quad (1)$$

The corresponding phase curve for the RVs of Table 3 is shown in Fig. 3.

Next we folded the Hα and Hβ radial velocity samples (this time obtained with $FWHM_g$ = 4 (Hα) or 6 (Hβ) Å and Δ changing from 30 to 50 Å) with the ephemeris given in Eq. 1 and fit the phased radial velocity curves with sinusoids:

$$v_r = \gamma + Asin(2\pi\Phi) + Bcos(2\pi\Phi) \quad (2)$$

where Φ is the phase, γ the zero point and A and B coefficients defining the radial velocity half-amplitude $K = \sqrt{A^2 + B^2}$.

The diagnostic diagrams for the Hα and Hβ emission lines are shown in Figs. 4 and 5. As occurs in many CVs, different $K - \gamma$ pairs are found depending on what part of the emission line is tested. The most important gradients are seen in Hα, where K changes from 50 km s^{-1} in the central parts of the profile to about 100 km s^{-1} in the wings. The same figure is almost constant (about 90 km s^{-1}) along most the Hβ profile. γ is also sensitive to the position in Hα, being anticorrelated with K, but is almost constant in Hβ. Finally we note that the shift with respect to the zero phase given by Eq. 1 (measured by $\Delta\Phi$) is almost zero for Hα and Hβ, this gives us confidence about the zero point of Eq. 1.

In order to find the best K value, we used the Schneider & Young's (1980) criterion, viz, the best estimate of K is provided at the largest Δ value, before σ_K/K starts to significantly increase. Here σ_K refers to the K error. This criterion is based on the belief that the wings are good tracers of the white dwarf motion. The best K values for Hα and Hβ are found at $\Delta = 47$ and 41 Å, respectively, i.e. around 2300 km s^{-1}. The results are summarized in Table 4. Both lines, Hβ and Hα, yield basically the same K value, viz. about 95 km s^{-1}, consistent with the 88 km s^{-1} value quoted by Ringwald (1993) (with and estimated error of 20 km s^{-1} from his Fig. 5.10).

We also intended to measure RVs for the other lines. In general, they were too noisy to give reliable results. Only for He 5875 we obtained a RV sample with a clear tendency. The ve-

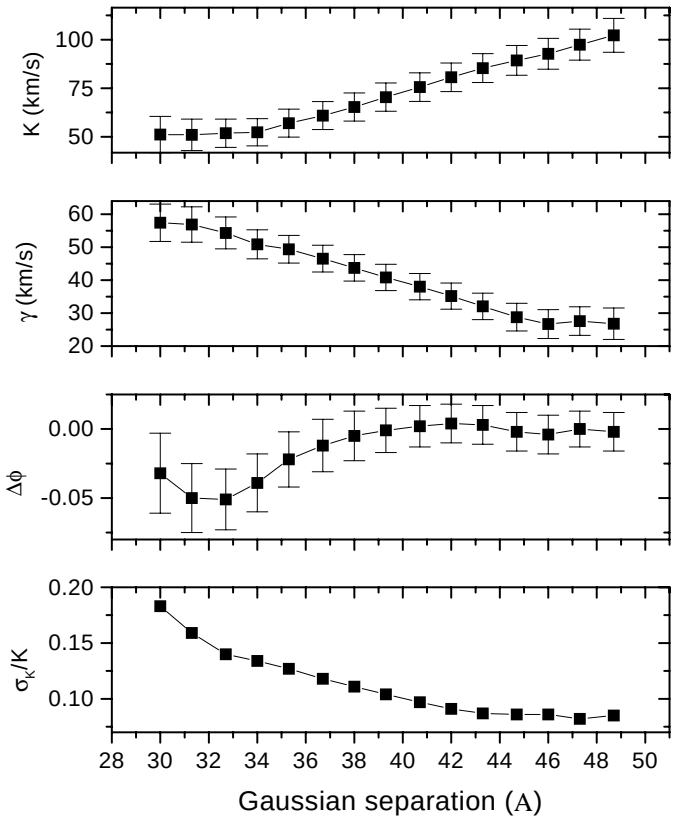

Fig. 4. The diagnostic diagrams for the Hα emission line.

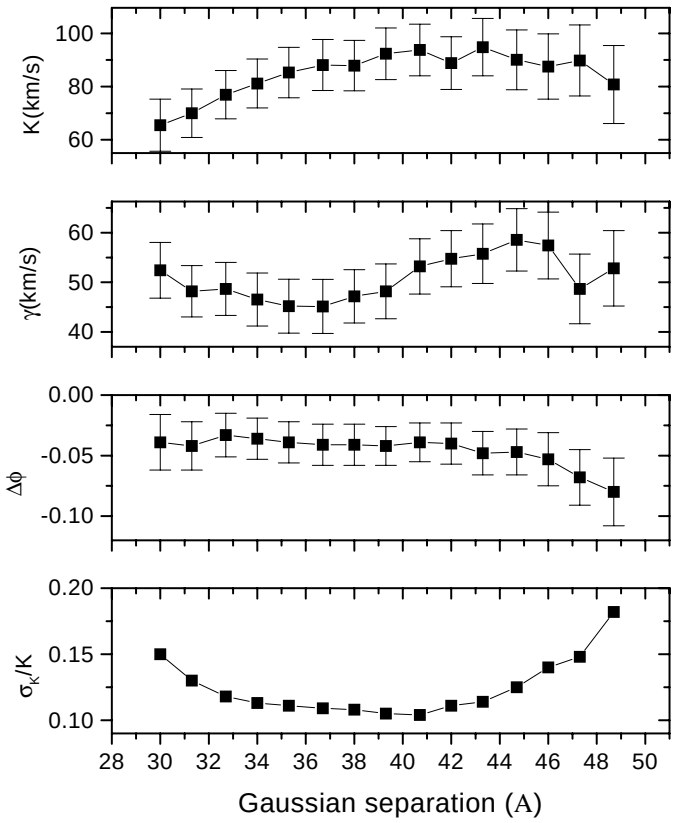

Fig. 5. The diagnostic diagrams for the Hβ emission line.

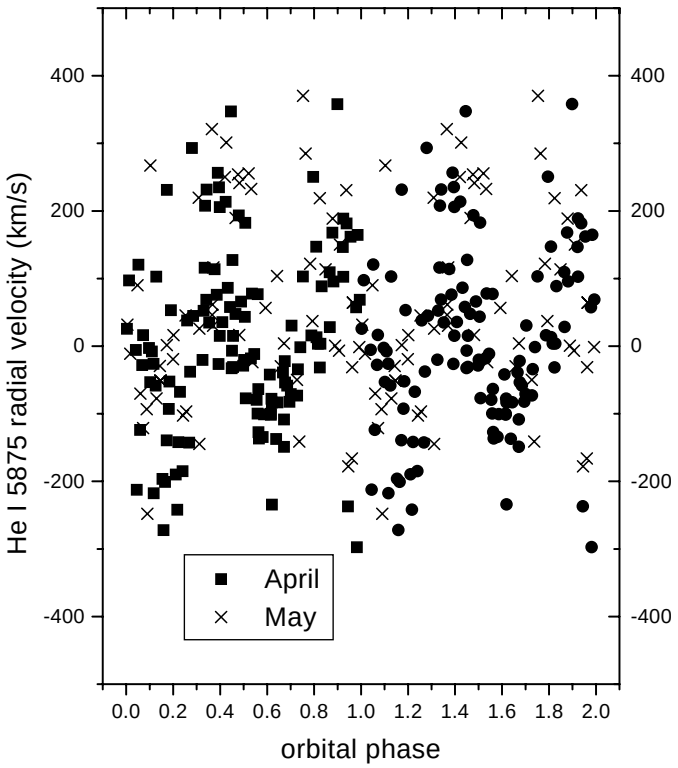

Fig. 6. The He I 5875 radial velocities folded with the orbital period $0.^{\rm d}07692$.

Table 4. Results of the diagnostic diagrams. The $K-\gamma$ values are given in km s^{-1}.

Line	K	γ	$\Delta\Phi$
Hα	97 ± 8	28 ± 4	0 ± 0.02
Hβ	94 ± 10	53 ± 6	-0.04 $\pm$ 0.02

locities, shown in Fig. 6 show a double wave. This phenomenon will be analyzed in detail in a subsequent paper.

4. Line radial emissivity gradients

We have measured the widths A_{84} ($\log W_{0.8}$ - $\log W_{0.4}$) and A_{41} ($\log W_{0.4}$ - $\log W_{0.1}$) for the emission lines of the average spectrum of April, where W represents the line width at a fraction of their maximum height.

Under some basic assumptions, the parameters A_{84} and A_{41} are good indicators of the disk line emissivity and disk radius. Assuming an axially symmetric, flat, Keplerian disk and a line emissivity $\propto r^{-t}$, Smak (1981) found a relationship between the pairs A_{84}–A_{41} and t–ρ, where $\rho \equiv \frac{r_{inn}}{r_{out}}$, is the ratio between the inner and outer disk radius. The mapping function resulted to be weakly dependent on the instrumental resolution, which he normalized to the peak's separation ($U = \frac{Res}{\Delta_\lambda}$).

We estimated t and ρ using our profile's measures and the Smak's (1981) Fig. 6, assuming that all line emissivity comes from the accretion disk. The results, given in Table 5, indicate a similar t for all lines with a mean 2.0 $\pm$ 0.2 (std). From the

Table 5. Emission line parameters (A), line emissivity gradients (t) and ratio ρ between the inner and outer disk radius.

Line	A_{41}	A_{84}	U	t	ρ
Hα	0.28(6)	0.24(4)	0.3	2.0(1)	0.035(13)
Hβ	0.22(5)	0.23(3)	0.2	2.1(1)	0.056(15)
He I 5875	0.22(4)	0.21(2)	0.1	2.0(1)	0.070(14)
He I 4471	0.12(3)	0.15(2)	0.1	2.0(1)	0.170(30)
He II 4686	0.13(4)	0.24(1)	0.1	2.3(2)	0.091(09)
He I 5015	0.32(3)	0.17(3)	0.1	1.7(2)	0.022(08)
He I 6678	0.12(2)	0.13(1)	0.1	1.8(2)	0.204(20)

ρ value of the Hα line, and using Eq. 4 by Mennickent & Arenas (1998), we estimated a supercycle length of 177 days, in agreement with the lower limit given by Kato et al. (1998).

The line emissivity in dwarf novae has been related to dissipation of magnetic energy in the disk (Horne & Saar 1991). As this kind of dynamo effect is known to be proportional to the angular velocity in stars with active chromospheres, and the disk angular velocity in a Keplerian disk is proportional to $r^{-3/2}$, the larger exponent found in the Balmer lines of dwarf novae could be evidence of deviations from pure Keplerian motion is their disks (Mennickent & Arenas 1998). This seems to be also applicable to HS Vir.

5. The "superhump" mass ratio and the $P_o - P_s$ relation in SU UMa stars

Before searching for the system parameters of HS Vir we will investigate a mass ratio estimator of general use among SU UMa stars.

Osaki (1985) derived an analytical expression for the precession rate of the eccentric keplerian orbit of matter at the disk's outer edge under the influence of the secondary's perturbing gravitational force:

$$\frac{\Omega_{pr}}{\Omega_o} = \frac{3}{4}\frac{q}{\sqrt{1+q}}(\frac{r_d}{a})^{3/2} \quad (3)$$

where Ω_{pr}, Ω_o, r_d and a are the precession and orbital frequencies, the disk outer radius and the semimajor axis of the circular orbit, respectively.

If the superhump frequency (Ω_s) reflects the displacement between the orbital and precession frequency, then:

$$\Omega_{pr} = \Omega_o - \Omega_s. \quad (4)$$

Combining the precession frequency and Eq. 3, defining the observable $\epsilon = \frac{(P_s - P_o)}{P_o}$ and assuming a disk radius equal to the 3:1 tidal resonance radius, i.e. about 0.46a (Whitehurst 1988a, Osaki 1989, Lubow 1991) we roughly obtain (e.g. Patterson 1998):

$$q = \frac{1}{0.23\epsilon^{-1} - 0.27}. \quad (5)$$

Due to the success of the tidal resonance model in reproducing the superhumps seen in SU UMa stars (e.g. Osaki 1985, Whitehurst 1988a,b, Hirose & Osaki 1990, Hirose et al. 1991, Lubow 1991, Whitehurst & King 1991, Lubow 1992, Hirose & Osaki 1993, Murray 1998), Eq. 5 seems to be a good tool for estimating the mass ratio in non eclipsing SU UMa stars. A test for Eq. 5 can be made with the data of the 4 eclipsing SU UMa stars for which independent mass ratios are available. The result of this comparison, given in Table 6, indicates that the model reproduces well the observed mass ratio, within the observational uncertainties.

Table 6. Comparison of observed (q_o) and predicted (q_{sh}, from Eq. 5) mass ratios. The ϵ parameter is from Patterson (1998) and references therein.

Star	ϵ	q_o	q_{sh}	Ref (q_o)
HT Cas	0.0330(30)	0.15(3)	0.149(14)	Horne et al. (1991)
OY Car	0.0203(15)	0.102	0.090(7)	Wood & Horne (1990)
Z Cha	0.0364(9)	0.15(3)	0.165(5)	Wade & Horne (1988)
WZ Sge	0.0080(6)	0.075(15)	0.035(3)	Spruit & Rutten (1998)

However, Eq. 5 was derived for one orbiting particle assuming gravity as the main driving force of precession, whereas the real phenomenon involves the collective motion of many particles probably influenced by pressure forces and viscosity (Murray 1998). Murray's main result is that ϵ is not only a function of the mass ratio (as previous studies suggested) but also a function of the gas pressure and viscosity. For example, ϵ increases by 15% when the gas pressure is incremented by a factor 5 in one of his simulations. This effect is of the same order that the ϵ changes observed during superoutburst for single systems, but it can also be explained uniquely as changes in disk radius through Eq. 3. This was done by Patterson et al. (1993) in order to explain the $\dot{P}_s \sim -6 \times 10^{-5}$ d/d commonly observed in SU UMa stars. Therefore, in our current stage of knowledge, we cannot discriminate between purely gravitational or physical causes for the ϵ changes.

As a working hypothesis we will assume that Eq. 5 is a first order approach to the mass ratio of SU UMa stars. We will call "superhump" mass ratio (q_{sh}) the mass ratio so derived. We estimate an intrinsic uncertainty $\epsilon_{q_{sh}} \approx 0.017\ \frac{q_{sh}^2}{\epsilon}$, obtained by propagating errors in Eq. 5 and assuming a typical ϵ variation of 15% through superoutburst.

Fig. 7 shows the q_{sh} and P_o distributions for the sample of the 39 SU UMa stars listed by Patterson (1998) and 4 additional stars (CU Vel Mennickent & Diaz 1996, EK TrA Mennickent & Arenas 1998, BR Lup Mennickent & Sterken 1998 and AK Cnc Arenas & Mennickent 1998). The q_{sh} distribution is well modeled with a gaussian function with a mean of 0.14 and standard deviation 0.05. This result is independent of the selected bin size. Extreme values are 0.04 (WZ Sge) and 0.34 (TU Men).[2]

[2] The main reason for including Fig. 7 is showing the sharp contrast between both distributions. Evidently, the sample is biased to high luminosity systems and an interpretation depends on a close comparison with realistic population synthesis models. These models should include CVs with He and CO white dwarfs as products of different initial conditions in the progenitors.

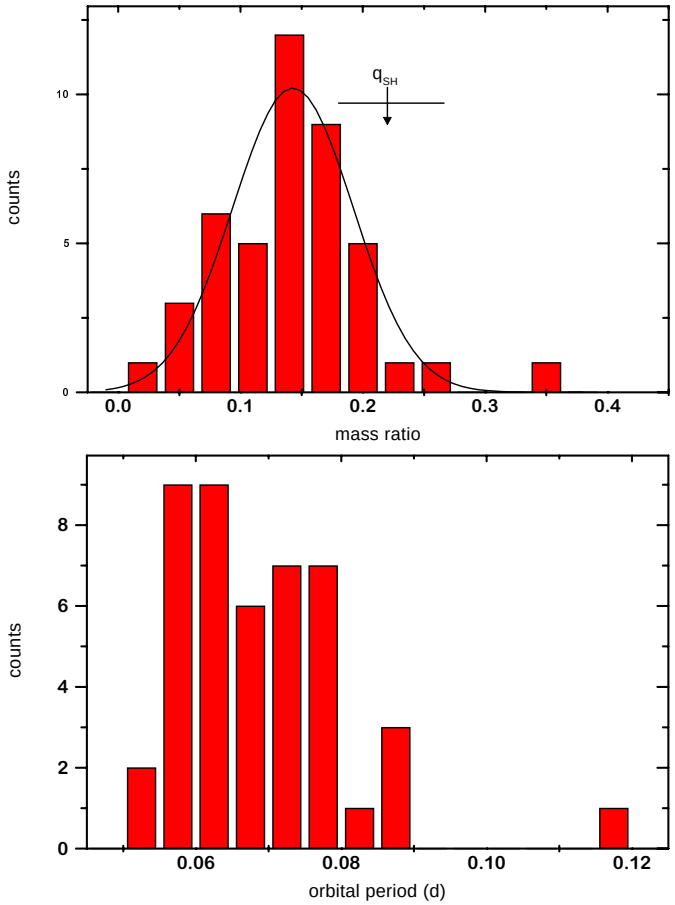

Fig. 7. The distributions of the orbital period and "superhump" mass ratio. All SU UMa stars in Patterson's (1998) Table 1 have been included, along with four additional stars (see text). Note the different shape of the q_{sh} distribution. The mass ratio of HS Vir derived from Eq. 5 is also shown.

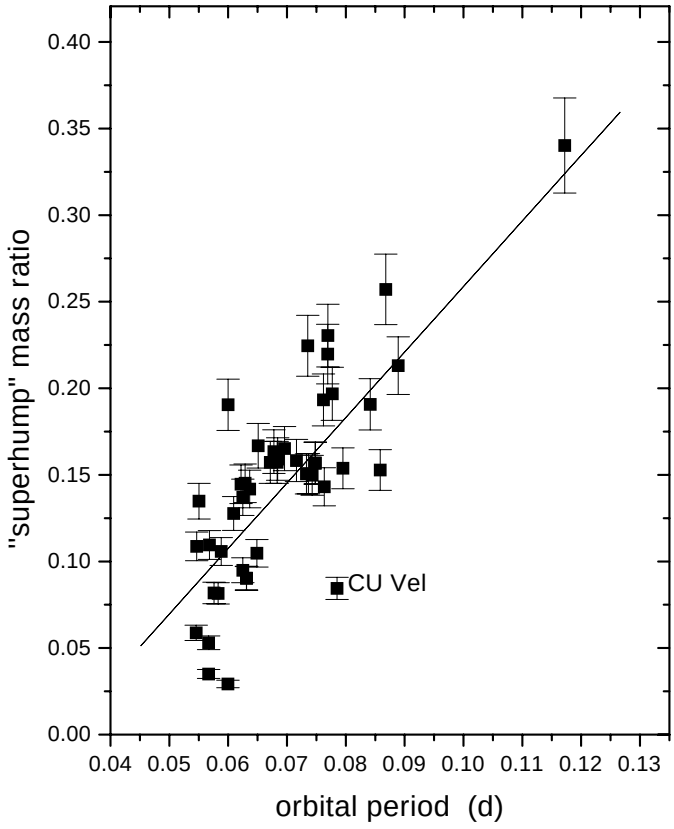

Fig. 8. The "superhump" mass ratio versus the orbital period. The best linear fit given by Eq. 6 is also shown along with estimated error bars. The outlier CU Velorum is labeled.

Figs. 8 and 9 show q_{sh} decreasing monotonically with the orbital period while P_o tightly follows P_s. Most of the scatter in these figures could be explained by the uncertainties associated to q_{sh} (already discussed) and the variation of the superhump frequency through superoutburst.[3] Least square fits were done for these data yielding the following equations:

$$q_{sh} = -0.11(3) + 3.8(5)P_o \quad (6)$$

with correlation coefficient 0.76 and std 0.04, and

$$P_o = 0\overset{\mathrm{d}}{.}0045(4) + 0.905(6)P_s \quad (7)$$

with correlation coefficient 0.999 and std 0.00057 d, in both cases the periods are in days.

The decrease of mass ratio with the orbital period indicated by Eq. 6 is expected from the standard scenario for the evolution of CVs below the period gap driven by angular momentum losses due to gravitational radiation (e.g. Kolb 1993).

On the other hand, Eq. 7 is a new version of the empirical relationship discovered by Stolz & Schoembs (1984) and improved by Howell & Hurst (1994) and Arenas & Mennickent (1998). Whereas the above authors used 7, 14, and 20 stars with known orbital and superhump periods respectively (actually Stolz & Schoembs calibrated ϵ vs. P_s) we have used 43 stars.

The $P_s - P_o$ relation is powerful for orbital period prediction; it easily discriminates between $\pm$ 1 c/d aliases which are commonly found in the literature of SU UMa stars. In fact, a typical orbital frequency of 16 c/d has $\pm$ 1 c/d aliases separated by $\pm\, 0\overset{\mathrm{d}}{.}004$ from the period. This value is one order of magnitude larger than the standard deviation associated to Eq. 7.

As an application of Eq. 5 and using ϵ = 0.0477(8) for HS Vir, we calculated a "superhump" mass ratio of 0.22(4), which is 2σ over the mean of the q_{sh} distribution (Fig. 9). This value compares well with the estimate from Eq. 6, viz. 0.18(4).

6. Possible system parameters

Using the empirical $M_2 - P_o$ relationship for near main sequence secondaries of cataclysmic variable stars by Warner

[3] CU Vel is an unique 7σ outlier in the range of long periods. This star also show a large deviation in the $P_o - P_s$ diagram (Fig. 9). The superhump period given by Vogt (1981) should be re-checked. The q_{sh} outliers at low periods (e.g. WZ Sge) have been interpreted as post-period minimum systems by Patterson (1998).

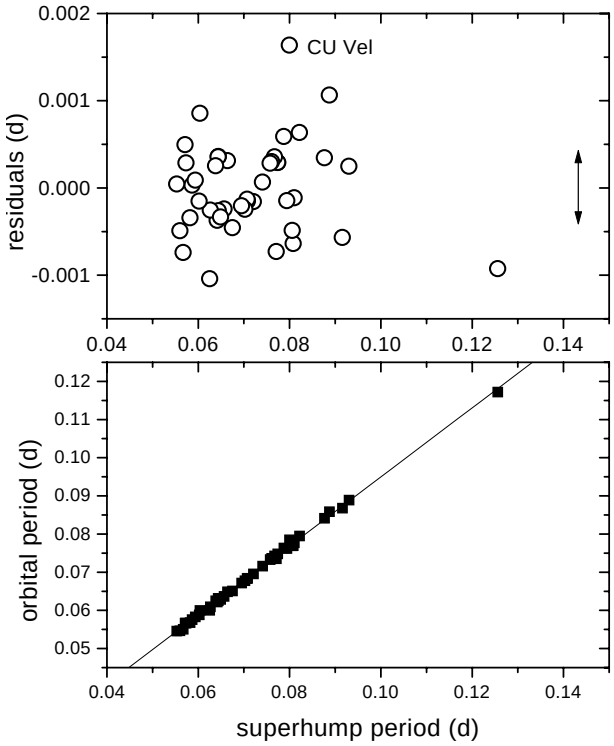

Fig. 9. The superhump period as a function of the orbital period. The best linear fit given by Eq. 7 along with their residuals (upper panel) are shown. The arrows indicate a typical variation of P_s through superoutburst. The outlier CU Velorum is labeled in the upper graph.

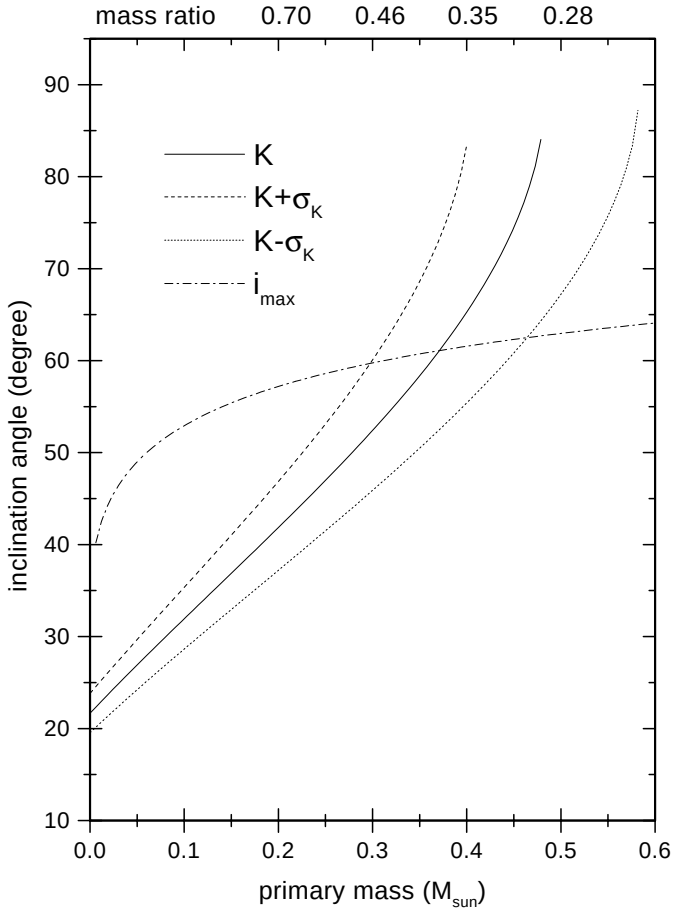

Fig. 10. The $i - M_1$ plane showing the dynamic solutions for the range of possible K (assuming M_2 = 0.14 $M_\odot$) and the maximum angle derived from the absence of eclipses. The upper horizontal axis is labeled with the mass ratio, indicating that $q \geq 0.37$ is needed to fulfill the observables K and P_o.

(1995b, Eq. 2.100):

$$M_2 = 0.065\ P_o^{5/4} M_\odot \ \ 1.3\ hr\ \leq P_o \leq\ 9\ hr \tag{8}$$

we find $M_2 = 0.140 M_\odot$ (0.131 $M_\odot$ using Eq. 5 by Patterson 1998). The observables K (the mean of the Balmer line values, i.e. $96 \pm 9\,\mathrm{km\,s^{-1}}$) and P_o provide strong constraints on the stellar masses and systemic inclination through the mass function:

$$2\pi G M_1 \sin^3 i = P_o K^3 \frac{(1+q)^2}{q^3} \tag{9}$$

In addition, as the system is not eclipsing (Howell et al. 1990), we can get an upper limit for the inclination. For that we used the Eggleton (1983) approximation for the volume Radius $R_L(2)$ of the Roche lobe of the secondary star, obtaining:

$$\begin{aligned} \tan^{-1} i_{max} &= \frac{R_L(2)}{a - r_d} \\ &= \frac{0.49 q^{2/3}}{(1 - r_d/a)[0.6 q^{2/3} + \ln(1 + q^{1/3})]} \end{aligned} \tag{10}$$

Assuming a disk radius equal to $0.46a$, an upper limit $i_{max} \approx 60^o$ is found, basically independent of q. In addition, the condition that the $HWZI$ of the emission lines cannot be greater than the Keplerian velocity corresponding to the primary radius, combined with the white dwarf mass-radius relation by Nauenberg (1972) yields $M_1 > 0.43\ M_\odot$. For that we used the mean $FWZI$ of the values listed in Table 2, viz. $3770\,\mathrm{km\,s^{-1}}$. Due to the large scatter in $FWZI$ values, this is a rather uncertain limit.

The dynamical solution, shown in Fig. 10, indicates $M_1 < 0.38\ M_\odot$ and $q > 0.37$. This is almost 4σ over the q based on Eq. 5. Moreover, it is incompatible with previous work indicating that the superhump phenomenon develops just in low mass ratio systems (with roughly $q \leq 0.33$, e.g. Whitehurst 1988a, Whitehurst & King 1991). We have two alternatives to explain this controversy: or q_{sh} does not represent the true mass ratio or the dynamic solution is corrupted by a wrong K value. Up to now, the evidence shown in Table 6 and the observations of variable K in other dwarf novae (e.g. TY PsA, O'Donoghue & Soltynski 1992) favor the last alternative.

7. Conclusions

– The most likely orbital period of HS Vir, viz. $0^{\mathrm{d}}.07692(3)$ has been determined from a study of the radial velocities of the Balmer emission lines. Two aliases at $0^{\mathrm{d}}.07678$ and $0^{\mathrm{d}}.07709$ cannot be completely discarted.

– The radial velocities of the He I 5875 double emission line show a double wave during the orbital cycle.
– Emissivity gradients $\propto r^{-t}$ of the main emission lines were determined, yielding a mean $t = 2.0 \pm 0.2$ (std).
– A revised version of the $P_o - P_s$ relation is given. We remark their importance as an estimator of the orbital period discriminating between $\pm$ 1 c/d aliases (Eq. 7).
– The mass ratio distribution of SU UMa stars, as derived from the tidal resonance model, has a roughly gaussian shape with a mean 0.14 contrasting with the orbital period distribution. A close comparison with population synthesis models and a proper treatment of selection effects is needed to establish the implications of this finding.
– The "superhump" mass ratio of HS Vir (0.22) is in disagreement with the figure derived from the dynamic solution. The radial velocity semi-amplitude, derived from the emission lines, could not reflect the motion of the white dwarf around the center of mass of the binary.

Acknowledgements. We thank Dr. S. Howell by useful discussions about CV evolution. This work was partly supported by Fondecyt 1971064 and DI UdeC 97.11.20-1. Support for this work was also provided by the National Science Foundation through grant number GF-1002-98 from the Association of Universities for Research in Astronomy, Inc., under NSF Cooperative Agreement No. AST-8947990. J.A. acknowledges support by a Gemini-PPARC-FANDES studentship and O.R.S. award. K.M. acknowledges the Hayakawa-Yukio Foundation of the Astronomical Society of Japan.

References

Arenas J., Mennickent R.E., 1998, A&A 337, 472
Echevarría J., 1988, MNRAS 233, 513
Eggleton P.P., 1983, ApJ 268, 368
Ferguson D.H., 1997, ApJ 486, 987
Hirose M, Osaki Y., 1990, PASJ 42, 135
Hirose M., Osaki Y., Mineshige S., 1991, PASJ 43, 809
Hirose M., Osaki Y., 1993, PASJ 45, 595
Hoare M.G., 1994, MNRAS 267, 153
Horne K., Wade R.A., Szkody P., 1986, MNRAS 219, 791
Horne K., Saar S.H., 1991, ApJ 374, 55
Horne K., Wood J.H., Stiening R.F., 1991, ApJ 378, 271
Howell S.B., Szkody P., Kreidl T.J., Mason K., Puchnarewicz E., 1990, PASP 102, 758
Howell S.B., Hurst G.M., 1994, IBVS 4043
Kato T., Nogami D., Masuda S., Hirata R., 1995, IBVS 4193
Kato T., Nogami D., Baba H., 1996, PASJ 48, L93
Kato T., Nogami D., Masuda S., Baba H., 1998, PASP 110, 1400
Kolb U., 1993, A&A 271, 149
Lubow S.H., 1991, ApJ 381, 268
Lubow S.H, 1992, ApJ 401, 317
Mennickent R.E., Diaz M., 1996, A&A 309, 147
Mennickent R.E., Arenas J., 1998, PASJ 50, 333
Mennickent R.E., Sterken C., 1998, PASP 110, 1032
Misselt K.A., Shafter A.W., 1995, AJ 109, 1757
Murray J.R., 1998, MNRAS 297, 323
Nauenberg M., 1972, ApJ 175, 417
Nogami D., Kato T., Masuda S., et al., 1995, PASJ 47, 897
O'Donoghue D., Soltynski M.G., 1992, MNRAS 254, 9
Osaki Y., 1985, A&A 144, 3690
Osaki Y., 1989, PASJ 41, 1005
Patterson J., 1998, PASP 110, 1132
Patterson J., Bond H.E., Grauer A.D., Shafter A.W., Mattei J.A., 1993, PASP 105, 69
Ringwald F.A., 1993, Ph.D. Thesis, Dartmouth Coll., Hanover, N.H.
Ritter H., Kolb U., 1998, A&AS 129, 83
Robertson J.W., Honeycutt R.K., Turner G.W., 1995, PASP 107, 443
Scargle J.D., 1982, ApJ 263, 835
Schneider D.P., Young P., 1980, ApJ 238, 946
Shafter A.W., 1983, ApJ 267, 222
Smak J., 1981, Acta Astron. 31, 395
Sperl M., 1998, http://dsn.ast.univie.ac.at/ period98/
Spruit H.C., Rutten R.G.M., 1998, MNRAS 299, 768
Stellingwerf R.F., 1978, ApJ 224, 953
Stolz B., Schoembs R., 1984, A&A 132, 187
Vogt N., 1981, Habilitation Thesis, Bochum University
Wade R.A., Horne K., 1988, ApJ 324, 411
Warner B., 1995a, A&SS 226, 187
Warner B., 1995b, Cataclysmic Variable Stars. Cambridge University Press
Whitehurst R., 1988a, MNRAS 233, 529
Whitehurst R., 1988b, MNRAS 232, 35
Whitehurst R., King A., 1991, MNRAS 249, 25
Williams R.E., Ferguson D.H., 1982, ApJ 257, 672
Wood J.H., Horne K., 1990, MNRAS 242, 606